Atomic and magnetic short-range order in a Pt−8.8 at. % Mn spin-glass alloy

Miwako Takahashi, Syunji Yoshimi, and Ken-ichi Ohshima
Institute of Applied Physics, University of Tsukuba, Tsukuba 305-8573, Japan

Yousuke Watanabe
Institute for Materials Research, Tohoku University, Sendai 980-8577, Japan
(Received 9 March 1999; revised manuscript received 23 August 1999)

The x-ray and neutron diffuse scattering intensities from a disordered Pt−8.8 at. % Mn spin-glass alloy were measured to obtain information about structural fluctuations due to atomic and magnetic short-range order. Diffuse maxima have been observed at the (100), (110) and their equivalent positions. Additional diffuse scatterings are also found at (1/2,1/2,1/2) and its equivalent positions on the x-ray and neutron diffraction patterns at room temperature. Warren-Cowley atomic short-range order (ASRO) parameters were obtained by analyzing the x-ray diffuse intensity data. The correlation length has been deduced to be about 15 Å from estimating the reconstructed diffuse intensity distribution using the ASRO parameters determined experimentally. The neutron scattering result shows that a magnetic diffuse maximum appears at around (1/2,0,0). The magnetic peak disappears at temperature far above the freezing temperature T_g at which a cusp-type peak is observed in the magnetic susceptibility measurement. The origin of the diffuse scattering is discussed in terms of a spin-density wave (SDW) induced by a Fermi surface nesting effect. The spin-glass-like behavior of Pt-Mn alloys is interpreted by the model of dynamically fluctuating SDW clusters as proposed for other metallic spin-glass alloys.

I. INTRODUCTION

The Pt-Mn alloy system exhibits a wide variety of magnetic properties as the Mn concentration is changed. The Pt-rich Pt-Mn alloy system has a fcc structure above the order-disorder transition temperature T_c, and a Cu_3Au-type chemical-order phase, which is stable in the range 17–27 at. % Mn below T_c. The ordered Pt_3Mn alloy is ferromagnetic below $T_c = 390$ K with a well-localized magnetic moment of $\mu_{Mn} = 3.64\mu_B$ and $\mu_{Pt} = 0.26\mu_B$.[1] On the other hand, Pt-Mn alloys with lower Mn concentrations are regarded as prototypes of spin-glass behavior, similar to the Cu-Mn alloy system that has long been known as a typical spin-glass. The studies on the spin-glass Pt-Mn alloys have concentrated on dilute alloys of less than 3 at. % Mn.

Nieuwenhuys *et al.*[2] measured the magnetic specific heat of Pt–0.36, –0.88, and –1.64 at. % Mn alloys and found typical spin-glass behavior, with a pronounced maximum in the temperature dependence of the specific heat, the maximum temperature T_{max} scaling roughly with the Mn concentration. Sacli *et al.*[3] measured the magnetic specific heat of Pt–0.26, –0.47, –0.67, –0.97, and –1.35 at. % Mn alloys. They found indications of antiferromagnetic ordering below 0.8 at. % Mn and ferromagnetic ordering for higher concentration. Kimishima *et al.*[4] measured the magnetic specific heat of Pt–1.0, –2.0, and –2.6 at. % Mn alloys. They found that the magnetic specific heat was proportional with temperature for $T < T_{max}$ as in the case of canonical spin-glass Cu-Mn alloys. However, the slope of the specific heat in the linear range was decreasing with increasing Mn content, which has not been observed in other spin-glass alloys. They also found the presence of an energy gap at low temperature. They tried to understand the results through the presence of diffusive ferromagnetic spin waves.

Sarkissian *et al.*[5] measured the electrical resistivity for 0.5–18 at. % Mn down to about 30 mK. They found a pronounced minimum in the temperature dependence of the magnetic resistivity up to 11 at. % Mn. The behavior is in contrast to the other spin-glasses, where a maximum in resistivity is observed. Above 11 at. % Mn, there is no minimum and the resistivity is found to increase monotonically with increasing temperature. However, they found that the behavior of the resistivity of 12 at. % Mn alloy changes with heat treatments of the sample and pointed out the importance of atomic short-range order (ASRO) above 11 at. % Mn. Kästner *et al.*[6] measured the electrical resistivity for Pt–0.05, –0.2, –0.25, –0.50, and –1.0 at. % Mn alloys in a temperature range from 0.05 to 10 K. They found that the temperature of minimal resistivity was proportional to the Mn content. They interpreted the resistivity behavior in terms of the cluster model.

In susceptibility and magnetization measurements, typical spin-glass features, i.e., the cusp anomaly at the freezing temperature T_g in susceptibility and remanent magnetization below T_g, are observed in a wide concentration range of disordered Pt-Mn alloys. Tholence and Wassermann[7] measured the magnetic susceptibility for Pt–0.05, –0.1, and –0.25 at. % Mn alloys. They found that although very dilute Pt-Mn alloys with Mn concentrations below 0.05% show Kondo behavior with a Kondo-temperature on the order of 25 mK, samples above 0.1 at. % Mn show spin-glass characteristic features at low temperature. Further, Wassermann[8] determined the composition dependence of T_g up to the concentrated composition region, 15 at. % Mn. He showed that T_g increases continuously with increasing Mn concentration up to $T_g = 27.5$ K for 15 at. % Mn. On the other hand, the paramagnetic Curie temperature Θ increases in negative values up to 10 at. % Mn and then changes drastically from

−45 K at 10 at. % Mn to 100 K at 15 at. % Mn. He related the ferromagnetic interaction in 15 at. % Mn to the contributions of ferromagnetic Pt_3Mn. In contrast, antiferromagnetic ordering at lower Mn concentration was attributed to the oscillating Ruderman-Kittel-Kasuya-Yosida interaction. He also insisted that a transition from cluster glass with preferably antiferromagnetic order to a mixed ferromagnetic and antiferromagnetic-ordered cluster glass occurs at around 13 at. % Mn. The above results suggest that the ASRO has a strong effect on the magnetic behavior for the concentrated composition region.

A quantitative study for ASRO has been tried only for 8 at. % Mn by Morgownik and Mydosh.[9] From the neutron scattering measurement, they found diffuse intensity maxima at the (100) and (110) reciprocal lattice positions due to ASRO on a polycrystalline sample with 8 at. % Mn. They determined the first two Warren-Cowley ASRO parameters: $\alpha_1 = -0.056$ and $\alpha_2 = 0.047$. The correlation length was estimated to be about 10 Å . However, the ASRO diffuse intensity distribution on the reciprocal lattice plane was not shown because a polycrystalline sample was used in their study.

Recent neutron-scattering measurements have revealed that spin-glass behavior for many metallic spin-glass alloys, such as Cu-Mn, Ag-Mn, Pd-Mn, and Pd-Cr, is explained by the formation of spin-density-wave (SDW) clusters induced by a Fermi surface nesting effect.[10,11] In Cu-Mn alloys, magnetic satellite diffuse peaks are observed at $(1,1/2+\delta,0)$ with a strong inelastic component that persists far above T_g.[10] This fact indicates that the SDW clusters fluctuate dynamically above T_g, and play an essential role in spin-glass behavior.

In this paper we report the following experimental results from a single crystal of disordered Pt–8.8 at. % Mn alloy. First, we observe a weak diffuse maxima at (1/2,1/2,1/2) and equivalent positions, in addition to the above-mentioned diffuse maxima in the x-ray and neutron-diffraction patterns at room temperature, which originate from atomic short-range order. We determine the first 31 ASRO parameters experimentally, necessary to reconstruct both diffuse scatterings. Finally, we report the appearance of magnetic diffuse maxima at (1/2,0,0) and equivalent positions on the neutron-diffraction pattern below 150 K and the parameters related to the magnetic properties.

II. SAMPLE PREPARATION

A single crystal was grown using the Bridgman technique in a high-purity alumina crucible at the Institute for Materials Research, Tohoku University. A sample slice for x-ray diffuse-scattering experiments was cut parallel to a (210) plane with a diameter of 12 mm from the original single crystal ingot. The slice was polished mechanically and etched electrically to remove the distorted surface layer with the use of an electrolyte containing 20% H_2SO_4 and 80% distilled water, at room temperature. A cylindrical sample of 12 mm in diameter and 10 mm height for neutron study was cut from the same ingot. In order to measure the magnetic susceptibility, a sample with dimensions of $5\times5\times1$ mm^3 was also cut from the ingot. All the samples were annealed in an evacuated silica tube at 800 °C for 120 h and gradually cooled to room temperature. The surface of the specimen was etched electrically again to remove the oxide layer. The composition of the sample was determined by an electron probe microanalysis (EPMA) technique at the Chemical Analysis Center, University of Tsukuba. Data were taken from ten different spots of a given sample and the average value of these ten spots data was considered as the composition of that sample. Pure Pt and Mn were used as the standard materials for the EPMA experiment. The composition of the specimen is $x = 0.088 \pm 0.002$ in the $Pt_{1-x}Mn_x$ alloy system.

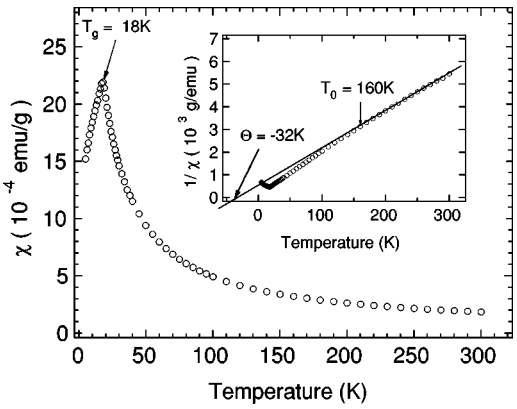

FIG. 1. Temperature dependence of the dc magnetic susceptibility of a Pt–8.8 at. % Mn alloys as measured by a SQUID in a field of 100 Oe with zero-field cooling. The insert shows the inverse magnetic susceptibility $1/\chi$ vs temperature.

III. MAGNETIC SUSCEPTIBILITY MEASUREMENTS

The magnetic susceptibility measurements were carried out using a superconducting quantum interference device (SQUID) in the temperature range 5 to 300 K.

Figure 1 shows the magnetic susceptibility $\chi(T)$ as measured in a 100 Oe magnetic field after zero-field cooling. We observe a cusp-type peak at the freezing temperature T_g ($=18$ K) and a remanent magnetization below T_g, which is a typical spin-glass behavior. The insert of Fig. 1 shows the inverse of $\chi(1/\chi)$ versus temperature T. The paramagnetic susceptibility deviates from the Curie-Weiss law below $T_0 = 160$ K. The paramagnetic Curie temperature Θ obtained as the extrapolated value at $1/\chi = 0$ is -32 K. The negative value of Θ indicates that antiferromagnetic interactions dominate in the specimen. The corresponding value of the effective number of Bohr magnetons p_{eff} calculated from the slope of $1/\chi(T)$ plot above T_0 is $5.95\mu_B$. These values are consistent with previous data.[8]

IV. X-RAY EXPERIMENTS AND RESULTS

The x-ray intensity measurement was performed at room temperature by using a four-circle goniometer attached to the rotating anode of an x-ray generator (Rigaku, RU-300). The incident beam, Cu $K\alpha$ from a Cu target, was monochromatized by a highly oriented pyrolytic graphite crystal. We introduced a high-performance x-ray detector using a $3\times3\times2$ mm^3 $Cd_{0.9}Zn_{0.1}Te$ (CZT) with preamplifier and cooler system (XR-100T-CZT, Amptek Inc.). The detector is so compact and light that it is easy to mount on the usual

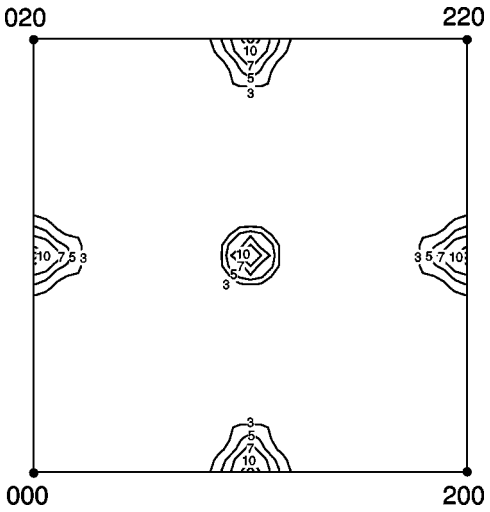

FIG. 2. The atomic short-range order component of diffuse intensity in the (001) scattering plane in Laue units for Pt–8.8 at. % Mn alloy.

counter arm without any difficulty. This has two main advantages over a conventional scintillation counter, twice the energy resolution and one-tenth the background. This detector is far more effective for measuring diffuse scattering intensity than the conventional one.

The x-ray diffuse scattering intensity measurement of the Pt–8.8 at. % Mn alloy was performed. Figure 2 shows the ASRO diffuse intensity distribution in the (001) scattering plane in Laue units. The contributions of the size-effect modulation, temperature-diffuse scattering, Huang scattering, Compton scattering, and air scattering have been subtracted. Diffuse maxima are clearly observed at (100), (110) and equivalent positions (X point of the fcc Brillouin zone). Figure 3 shows the ASRO diffuse intensity distribution in the $(1\bar{1}0)$ scattering plane in Laue units. Additional diffuse maxima appear at (1/2,1/2,1/2) and equivalent positions (L point of the fcc Brillouin zone) in addition to the diffuse scattering at the X point, though the intensity of the diffuse maximum at the (1/2,1/2,1/2) position is only about 30% of the (100) position.

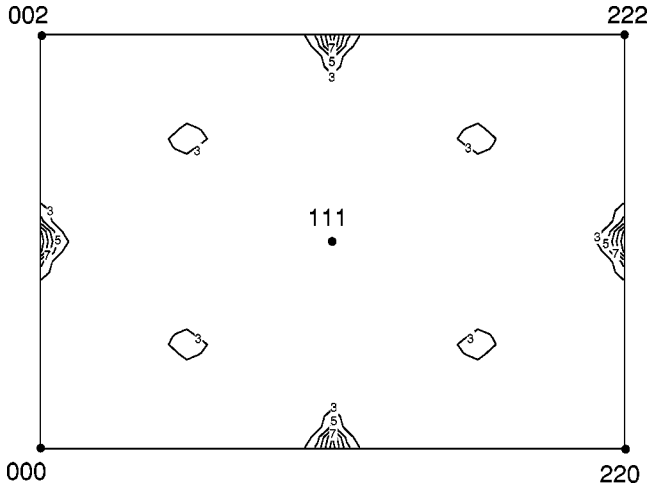

FIG. 3. The atomic short-range order component of diffuse intensity in the $(1\bar{1}0)$ scattering plane in Laue units for Pt–8.8 at. % Mn alloy.

TABLE I. ASRO parameters α_{lmn} for Pt–8.8 at. % Mn alloy determined from the Fourier transform of the ASRO diffuse intensities where N is the shell number.

N	lmn	α_{lmn}	N	lmn	α_{lmn}
	000	0.978	30	800	−0.002
1	110	−0.040	31	554	0.002
2	200	0.021		741	0.003
3	211	−0.018		811	−0.006
4	220	0.068	32	644	0.000
5	310	−0.012		820	0.002
6	222	0.015	33	653	−0.003
7	321	−0.003	34	660	0.006
8	400	0.042		822	0.008
9	330	0.001	35	743	0.002
	411	−0.014		750	−0.007
10	420	0.010		831	−0.005
11	332	−0.014	36	662	0.001
12	422	0.026	37	752	0.008
13	431	−0.009	38	840	−0.001
	510	0.001	39	833	−0.006
14	521	−0.007		910	0.008
15	440	0.017	40	842	0.004
16	433	−0.001	41	655	−0.004
	530	−0.002		761	−0.003
17	442	0.005		921	−0.001
	600	−0.006		664	0.009
18	532	0.001	43	754	−0.007
	611	−0.004		930	0.002
19	620	0.014		851	−0.002
20	541	0.000	44	763	−0.005
21	622	0.002		932	0.002
22	631	−0.005	45	844	0.009
23	444	0.018	46	770	0.004
24	543	−0.003		853	−0.005
	550	0.001		941	−0.001
	710	0.000	47	860	0.011
25	640	0.000		1000	−0.005
26	552	−0.012	48	772	−0.001
	633	−0.008		1011	−0.010
	721	0.002	49	862	0.002
27	642	0.013		1020	0.002
28	730	−0.001	50	943	−0.002
29	651	−0.003		950	0.007
	732	−0.005			

The ASRO diffuse intensity $I_{\mathrm{ASRO}}(\boldsymbol{q})$ at the scattering vector $\boldsymbol{q}$ can be written as follows:

$$I_{\mathrm{ASRO}}(\boldsymbol{q}) = N I_{\mathrm{laue}} \alpha(\boldsymbol{q}), \tag{1}$$

$$\alpha(\boldsymbol{q}) = \sum_{lmn} \alpha(\boldsymbol{R}_{lmn}) \exp(i \boldsymbol{R}_{lmn} \cdot \boldsymbol{q}), \tag{2}$$

$$I_{\mathrm{laue}} = c(1-c)(f_{\mathrm{Pt}} - f_{\mathrm{Mn}})^2, \tag{3}$$

$$\boldsymbol{R}_{lmn} = l\boldsymbol{a}/2 + m\boldsymbol{b}/2 + n\boldsymbol{c}/2, \tag{4}$$

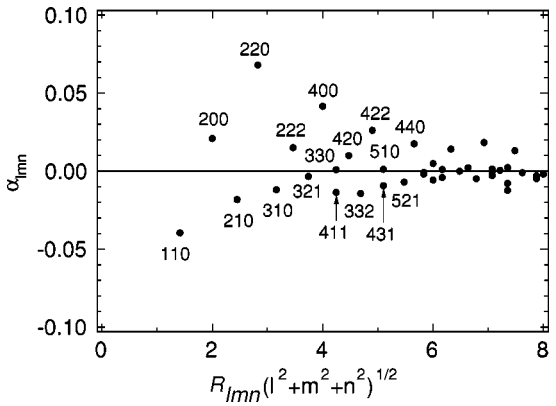

FIG. 4. Atomic short-range order parameters α_{lmn} plotted against R_{lmn} for Pt–8.8 at. % Mn alloy, where l, m, and n are integers.

where N is the number of atoms in the sample, f_{Pt} and f_{Mn} are the atomic-scattering factor of Pt and Mn atoms, c is the Mn concentration and $(\boldsymbol{a},\boldsymbol{b},\boldsymbol{c})$ are the basic vectors of the fcc lattice. α is the Warren-Cowley ASRO parameter and the parameter for nth neighbor $\alpha(n)$ is defined as follows:

$$\alpha(n)=1-p_A(n)/x_A=1-p_B(n)/x_B, \tag{5}$$

where x_A and x_B represent the composition of A and B of a binary alloy with $x_A+x_B=1$ and

$$p_A(n)=\text{probability of finding an } A\text{atom}$$

$$\text{as a } \boldsymbol{r}_n \text{ neighbor of } B \text{ atom,}$$

$$p_B(n)=\text{probability of finding a } B \text{ atom}$$

$$\text{as a } \boldsymbol{r}_n \text{ neighbor of } A \text{ atom.}$$

The ASRO parameter α is negative when there is a preference for unlike neighbors, positive for like neighbors and zero for complete randomness. The ASRO parameters $\alpha_{lmn}=\alpha(\boldsymbol{R}_{lmn})$ for the Pt–8.8 at. % Mn alloy were determined from the experimental ASRO diffuse intensities up to the 50th shell and are listed in Table I, where l, m, and n are integers. The error was estimated to be less than 5%. To confirm the validity of the α parameters thus determined experimentally, the diffuse intensity map was synthesized using a limited number of those parameters. The first 31 α_{lmn} parameters are necessary to reconstruct the diffuse intensity distribution. It is therefore estimated that the correlation length is about 15 Å . The first 40 ASRO parameters versus distance R_{lmn} $[=(l^2+m^2+n^2)^{1/2}]$ are plotted in Fig. 4. As can be seen in the figure, the sign of the ASRO parameters is positive for all even indices (l,m,n) and are negative for mixed indices (l,m,n). The absolute values of the parameters have a tendency to become smaller with increasing distance. The sign of the first two parameters is the same as in the previous study,[9] but the amplitude is smaller.

V. NEUTRON EXPERIMENTS AND RESULTS

Neutron-scattering measurements for the Pt–8.8 at. % Mn alloy were carried out using the FOX spectrometer with a refrigerator installed, at the pulsed neutron-scattering facility

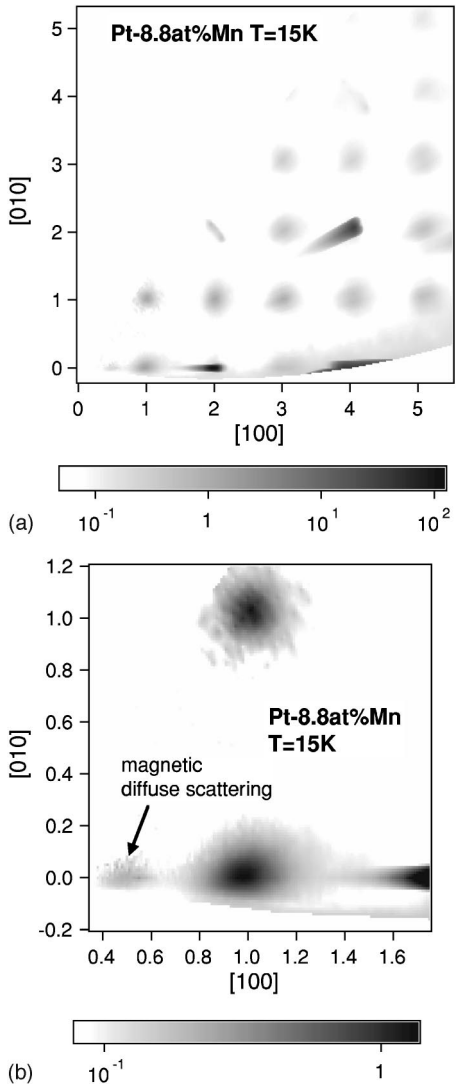

FIG. 5. (a) Neutron diffuse scattering intensity distributions in the (001) scattering plane and (b) an enlarged pattern of (a) around the (100) reciprocal lattice point.

of the High Energy Accelerator Organization, Tsukuba, Japan. The spectrometer is a single crystal diffractometer using the time-of-flight (TOF) Laue technique. The combination of the TOF technique with white neutrons, and a multidetector system of 36 linearly placed ^{3}He detectors makes it possible to observe a large area of reciprocal space in a single measurement. The instrument is ideal for reciprocal space surveying such as diffuse scattering studies or measurements of magnetic satellite peaks.

Figure 5(a) shows the intensity distribution in the (001) scattering plane of the Pt–8.8 at. % Mn alloy at 15 K. It took about 5 h to obtain one pattern. In the figure, TOF spectra were normalized with the incident neutron spectrum obtained by incoherent scattering from a vanadium specimen. Diffuse maxima are observed at (100) and equivalent positions, similar to the x-ray measurement. Figure 5(b) shows an enlarged pattern of Fig. 5(a) around the (100) reciprocal lattice point. We observe a broad diffuse maximum at (1/2,0,0). Since this was not seen by x-ray or neutron intensity measurements at room temperature, the diffuse scattering must be due to magnetic short-range ordering. The ratio of the

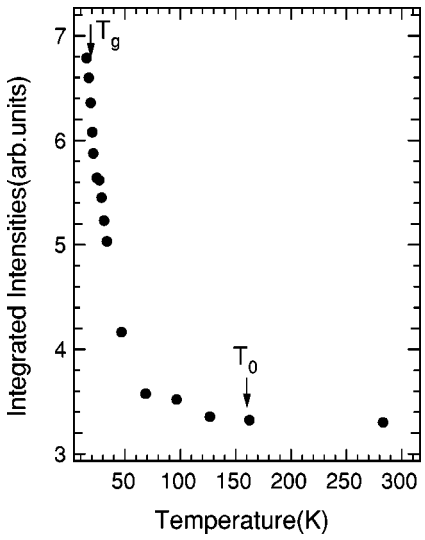

FIG. 6. Temperature dependence of integrated diffuse intensity at (1/2,0,0).

peak intensities at (200), (100), and (1/2,0,0) is about $10^2:1:10^{-1}$. The magnetic diffuse scattering is obtained by subtracting the intensity at room temperature from the observed intensity. This method has already been employed for selecting the magnetic diffuse intensity in an Ag–20.8 at.% Mn alloy.[12] The temperature dependence of the integrated diffuse intensities at (1/2,0,0) is plotted in Fig. 6 in a temperature range between 15 and 283 K. In the figure, arrows indicate T_g and T_0 as determined from magnetic susceptibility measurements at which the cusp-type anomaly and deviation from Curie-Weiss law are observed. The intensity begins to increase gradually as the temperature is lowered below T_0 and then increases more rapidly below 50 K, the temperature much higher than T_g. Furthermore, the temperature dependences of the position of the diffuse peak and the line width, which were determined by a Gaussian fit to the profile, are shown in Fig. 7 in a temperature range between 15 and 34 K. The position is almost temperature independent and the width decreases weakly with decreasing temperature.

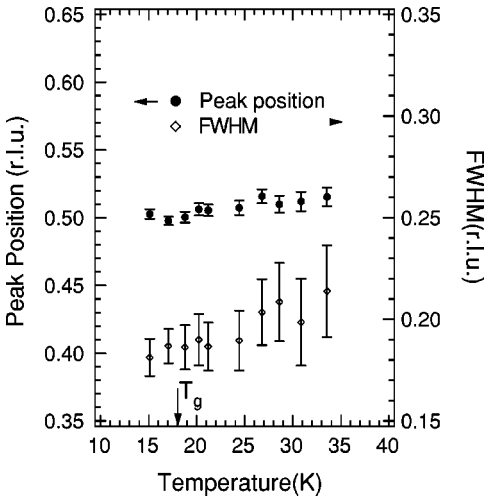

FIG. 7. Temperature dependence of the diffuse peak position and the linewidth, which are determined by Gaussian fits to the profile.

However, no anomaly at T_g is observed for the peak position or line width. The correlation length at T_g is about 20 Å, larger than that for the ASRO correlation length.

VI. DISCUSSIONS

From the present single crystal x-ray study, we have obtained more detailed information about the atomic short-range order (ASRO) than in the previous powdered neutron study.[9] Diffuse maxima at (1/2,1/2,1/2) and equivalent positions (L point) are observed in addition to the diffuse scattering at (100), (110) and equivalent positions (X point) in the x-ray diffraction pattern from a single crystal of the Pt–8.8 at.% Mn alloy. The diffuse maxima at the X point are due to the Cu_3Au-type ASRO. The diffuse maximum at the L point is due to the correlation between consecutive (111) planes of Pt or Mn atoms. The structure that has this type of correlation is known as CuPt-type structure. In our previous studies on Cu-Pt and Pd-Mn alloys, similar intensity distributions were observed.[13,14] In the case of the Cu-Pt alloy system, the CuPt-type ordered structure does exist for composition range from 28 to 93 at.% Pt. On the other hand, such an ordered structure does not appear in either the Pt-Mn or the Pd-Mn alloys system and there is no reason for the existence of this type of ASRO in these alloys. The correlation of the Cu_3Au-type ASRO requires that Mn atoms take predominantly corner positions in the fcc lattice, while that of the CuPt-type ASRO requires the corner positions to alternate between Pt and Mn atoms. Thus the sign and magnitude of α_{200} depends on the ratio of the L-point to the X-point diffuse maxima. In the case of Cu-Pt alloys, the ratio of the L- to the X-point diffuse intensities strongly depends on the composition and affects the sign and magnitude of (200).[13] In the present study, the sign of α_{200} is positive. We expect that the short-range ordered structure in the disordered Pt–8.8 at.% Mn alloy has a tendency to Cu_3Au-type ordering with the above layered correlation. To understand the origin of the Cu-Pt-type ASRO, a wide range of concentrations should be examined for the existence of such a structure.

The observed magnetic intensity at the (1/2,0,0) position indicates that the spin structure is modulated along the [100] direction with wavelength being twice as large as the chemical unit cell. The correlation length of the spin modulation below T_g, estimated from the line width at the (1/2,0,0) peak, is about 20 Å—five times larger than the chemical unit cell. The origin of the magnetic diffuse peak can be interpreted in terms of a Fermi-surface effect as proposed for other Pt-M and Pd-M (M is a $3d$ element) alloys.[11,15] In these alloys, satellite reflections are observed at the symmetry positions of $(1\pm\delta,0,0)$. The peak position δ varies continuously with the concentration of M, which is the result of the expansion of the Fermi surface of Pd and Pt due to the dilute addition of $3d$ ions. In our study, magnetic diffuse intensity at the (3/2,0,0) position was not detectable due to a much stronger tail of the (200) Bragg intensity and abrupt reduction of Mn^{2+} scattering length. The former is caused by an asymmetrical shape of the resolution of pulsed neutrons. The latter is a common feature of the magnetic neutron scattering. Since the intensities of magnetic scattering are governed by the form factor $f(q)$ of the spin polarized orbitals,

it approaches zero for large values of q. As for the scattering at (1/2,0,0), the observed peak position, $\delta = 0.5$, corresponds to the composition dependence in other Pt-M and Pd-M (M is a $3d$ element) alloys taken by Tsunoda *et al.*[11,15] The satellite peaks around the (100) reciprocal lattice point indicate that spin correlation is antiferromagnetic, which is consistent with the negative value of the paramagnetic Curie temperature Θ obtained by our susceptibility measurement.

The fact that the magnetic peak disappears far above T_g can be ascribed to the sufficiently broad energy resolution of the FOX spectrometer. Since we do not use a monochromator or an energy analyzer for the TOF method with white neutrons, the observed intensities include both elastic and inelastic components. On the other hand, dc magnetic susceptibility measures a completely static component. Thus, the intensities observed above T_g are considered to be inelastic intensities, suggesting that the modulated spin structure is not static but fluctuates in time. The observed temperature dependence of the magnetic peak profiles is very similar to those reported on Pd-Mn spin-glass alloys.[15] In the alloys, spin-glass behavior is explained using the model of dynamically fluctuating spin-density-wave clusters, originating from Fermi-surface nesting. The model was first proposed for the Cu-Mn alloy system and now is a common idea for metallic spin-glass alloys. In the study of Cu-Mn alloys, it was shown that the well-developed ASRO stabilizes the SDW formation.[16] At this point, we have to take the two types of observed ASRO into consideration to discuss the actual magnetic structure of disordered Pt-Mn alloys. On the other hand, since the ordered Pt_3Mn alloy with Cu_3Au-type structure is a simple ferromagnetic, competition between ferromagnetic order and the SDW formation in the Cu_3Au-type ASRO is expected for more concentrated Pt-Mn alloys. To confirm the above model based on a Fermi-surface effect and understand the relation between the two types of ASRO and magnetic structure in this system, measurements on the concentration dependence of both magnetic and atomic diffuse scatterings should be performed.

ACKNOWLEDGMENTS

We are grateful to K. Nishida of the Chemical Analysis Center, University of Tsukuba for his assistance in EPMA. We would like to express our thanks to the staff of the sample preparation room of the Institute for Materials Research, Tohoku University for help in preparing a single crystal. We are also grateful to M. Arai for his advice on neutron-scattering measurements, and A. Garrett for a careful reading of the manuscript. This work was partly supported by a grant from the Ministry of Education, Culture, Sports, and Science.

[1] B. Antonini, F. Lucari, F. Menzinger, and A. Paoletti, Phys. Rev. **187**, 611 (1969).
[2] G.J. Nieuwenhuys, M.F. Pikart, J.J. Zwart, B.M. Boerstoel, and G.J. Van den Berg, Physica (Amsterdam) **69**, 119 (1973).
[3] Ö.A. Sacli, D.J. Emerson, and D.F. Brewer, J. Low Temp. Phys. **17**, 425 (1974).
[4] Y. Kimishima, M. Kobayashi, R. Seto, and Y. Miyako, J. Phys. Soc. Jpn. **43**, 1577 (1977).
[5] B.V.B. Sarkissian and R.H. Taylor, J. Phys. F **4**, L243 (1974).
[6] J. Kästner, E.F. Wassermann, K. Matho, and J.L. Tholence, J. Phys. F **8**, 103 (1978).
[7] J.L. Tholence and E.F. Wassermann, Physica B&C **86-88**, 875 (1977).
[8] E.F. Wassermann, Physica B&C **109&110**, 1936 (1982).
[9] A.F.J. Morgownik and J.A. Mydosh, Solid State Commun. **47**, 325 (1983).
[10] J.W. Cable, S.A. Werner, G.P. Felcher, and N. Wakabayashi, Phys. Rev. B **29**, 1268 (1984).
[11] Y. Tsunoda, J. Magn. Magn. Mater. **177-181**, 1337 (1998).
[12] K. Koga, K. Ohshima, and N. Niimura, Phys. Rev. B **47**, 5783 (1993).
[13] D.K. Saha and K. Ohshima, J. Phys.: Condens. Matter **5**, 4099 (1993).
[14] D.K. Saha, K. Ohshima, M.Y. Wey, R. Miida, and T. Kimoto, Phys. Rev. B **49**, 15 715 (1994).
[15] Y. Tsunoda, N. Hiruma, J.L. Robertson, and J.W. Cable, Phys. Rev. B **56**, 11 051 (1997).
[16] Y. Tsunoda and J.W. Cable, Phys. Rev. B **46**, 930 (1992).